JOURNAL OF MATERIALS SCIENCE 23 (1988) 621–628

Creep rupture strength and grain-boundary sliding in austenitic 21Cr–4Ni–9Mn steels with serrated grain boundaries

MANABU TANAKA*, OHMI MIYAGAWA‡, TSUNEAKI SAKAKI‡, HIROSHI IIZUKA*, FUMIO ASHIHARA*, DAI FUJISHIRO§
*Department of Mechanical Engineering for Production, Mining College, Akita University, 1-1, Tegatagakuen-cho, Akita 010, Japan
‡Department of Mechanical Engineering, Faculty of Technology, Tokyo Metropolitan University, 2-1-1, Fukasawa, Setagaya-ku, Tokyo 158, Japan
§Nittan Valve Corporation Ltd, 2-7-2, Yaesu, Chuou-ku, Tokyo 104, Japan

The effect of grain-boundary strengthening on the creep-rupture strength by modification of the grain-boundary configuration is studied using austenitic 21Cr–4Ni–9Mn steel in the temperature range from 600 to 1000° C in air. Grain-boundary sliding is also examined on a steel with serrated grain boundaries during creep at 700° C. The improvement of creep-rupture strength by the strengthening of grain boundaries is observed at high temperatures above 600° C. The 1000 h rupture strength of steels with serrated grain boundaries is considerably higher than that of steels with straight grain boundaries, especially at 700 and 800° C. The strengthening by serrated grain boundaries is effective in retarding both the crack initiation and the crack propagation at 700° C, while it does not improve the life to crack initiation at 900° C. Grain-boundary sliding is considerably inhibited by the strengthening of grain boundaries at 700° C. The amount of it in steels with serrated grain boundaries is less than about one-third of that of steels with straight grain boundaries at the same creep strain. The stress dependence of grain-boundary sliding rate in the steady-state regime is also examined from the steels with these two types of grain-boundary configuration.

1. Introduction

The high-temperature strength of austenitic heat-resisting steels and nickel-base superalloys is considerably improved by the strengthening of grain boundaries [1–5]. The grain-boundary strengthening is usually achieved by slow cooling from solution temperature, which develops serrated grain boundaries caused by the formation of grain-boundary carbides or other precipitates [1, 6, 7].

The mechanism of grain-boundary strengthening has also been investigated for austenitic heat-resisting steels, and the strengthening by serrated grain boundaries is attributed to the retardation of grain-boundary sliding, which has an important role in grain-boundary fracture at high temperatures, the decrease in stress concentration at grain-boundary triple junctions with decreasing the length of sliding grain boundaries, and the occurrence of ductile grain-boundary fracture [8, 9]. It was also found as a result of analysis that the diffusion of atoms decreases the stress concentrations at grain-boundary triple junctions at high temperatures [10]. This may also lead to the retardation of triple-point cracking in materials with serrated grain boundaries compared with those with long, straight grain boundaries [10, 11]. However, the amount of grain-boundary sliding has not been measured on steels with serrated grain boundaries, and the quantitative relationship is not experimentally confirmed between the initiation and propagation of grain-boundary cracks and the grain-boundary sliding.

In this study, the creep rupture strength was investigated for austenitic 21Cr–4Ni–9Mn (wt %) heat-resisting steels with serrated grain boundaries and normal straight grain boundaries in the temperature range from 600 to 1000° C. An investigation was then made of the temperature dependence of grain-boundary strengthening effects in this kind of steel. Further, measurements of grain-boundary sliding in these steels were made to confirm the retardation effect of grain-boundary sliding by grain-boundary strengthening at 700° C.

TABLE I Chemical composition of steel used

	Composition (wt %)								
Steel	C	N	Cr	Ni	Mn	Si	S	P	Fe
21Cr–4Ni–9Mn	0.54	0.39	21.10	4.07	9.74	0.19	0.008	0.017	Balance

0022–2461/88 $03.00 + .12

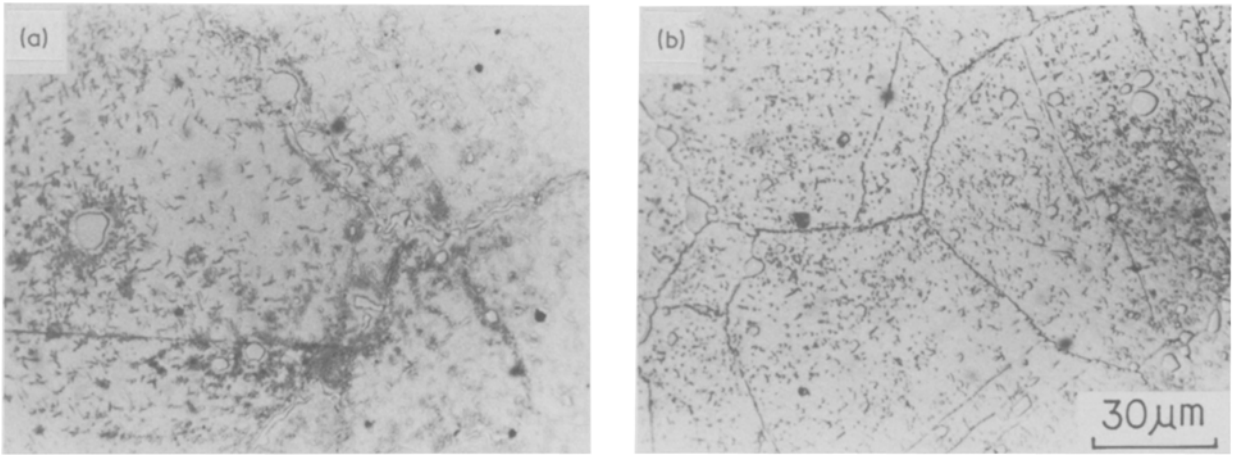

Figure 1 Optical micrographs of (a) Steel S, (b) Steel N.

2. Experimental procedure

Table I shows the chemical compositions of the austenitic 21Cr–4Ni–9Mn engine-valve steel with 16 mm diameter used in this study. The steel was heat-treated to obtain specimens with serrated grain boundaries (Steel S) and those with normal straight grain boundaries (Steel N) of the same hardness (about 320 H_V). Table II shows the heat-treatment procedure, and Fig. 1 shows microstructures of the steels. Steel S has serrated grain boundaries with coarse $M_{23}C_6$ grain-boundary carbides, while Steel N has straight grain boundaries with continuous carbides. The former steel has a grain-boundary length of about 5.72×10^{-5} m and the latter has a grain-boundary segment length of about 2×10^{-5} m, while both the steels have a same grain diameter of about 9.9×10^{-5} m.

Creep and creep-rupture tests were performed using the usual single-lever type of creep-rupture equipment with a capacity of 19.6 kN in the temperature range from 600 to 1000° C in air. Smooth round-bar specimens with 30 mm gauge length and 5 mm diameter were used for creep and creep-rupture experiments (Fig. 2a), and specimens with a transverse surface notch of 3 mm surface length (Fig. 2b) were employed for surface crack propagation experiments at 900° C.

Fig. 3 illustrates the technique of measuring the amount of grain-boundary sliding in the two kinds of steel at 700° C. Marker lines were scratched on the specimen surface with a knife-edge at a spacing of 0.2 or 0.3 mm. The average amount of grain-boundary sliding was obtained as a weighted mean value with sliding grain-boundary length from measurements of the off-set of marker lines (u) and the orientation of each grain boundary or grain-boundary segment (θ) after creeping specimens to a given strain [12]. The measurement of grain-boundary sliding was made on gold-coated surface replicas extracted from crept specimens with a scanning electron microscope.

The initiation of grain-boundary cracks on the creep and fracture surfaces of creep-ruptured specimens was examined with optical and scanning electron microscopes.

3. Results and discussions

3.1. Effect of grain-boundary strengthening on creep-rupture strength

Fig. 4 shows the creep-rupture strength of the steel with serrated grain boundaries (Steel S) and that with straight grain boundaries (Steel N) in the temperature range from 600 to 1000° C. Serrated grain boundaries improve the creep rupture strength at high temperatures above about 600° C. The 1000 h rupture strength of the steels with serrated grain boundaries is relatively higher than that of the steel with straight grain boundaries, especially at 700 and 800° C. Thus, it is obvious that the effect of grain-boundary strengthening is large at these temperatures.

Fig. 5 shows examples of creep curves for the steel with serrated grain boundaries and that with straight grain boundaries at 700° C. Arrows in the figure indicate the initiation of grain-boundary cracks. The steel with serrated grain boundaries has a longer rupture life and larger elongation than that with straight grain boundaries. Moreover, the time to crack initiation is also longer in the former. For example, the strain to crack initiation is 0.044 in the steel with serrated grain boundaries (Steel S) at 196 MPa, while it is 0.030 in the steel with straight grain boundaries at this stress. As will be seen later, grain-boundary cracks were initiated at the triple junctions [11, 13, 14] in the tertiary creep regime (about 80 to 90% of the rupture life) in these steels. The crack propagation period to rupture

TABLE II Heat treatment of steel

Specimens	Heat treatment*
Steel S (serrated grain boundaries)	1200° C × 1 h → F.C. → 1030° C → W.Q. + 750° C × 30 h → A.C. + 1000° C × 3 h → A.C.
Steel N (normal straight grain boundaries)	1200° C × 1 h → W.Q. + 700° C × 30 h → A.C. + 1000° C × 30 h → A.C.

*F.C. = furnace-cooled, W.Q. = water-quenched, A.C. = air-cooled.

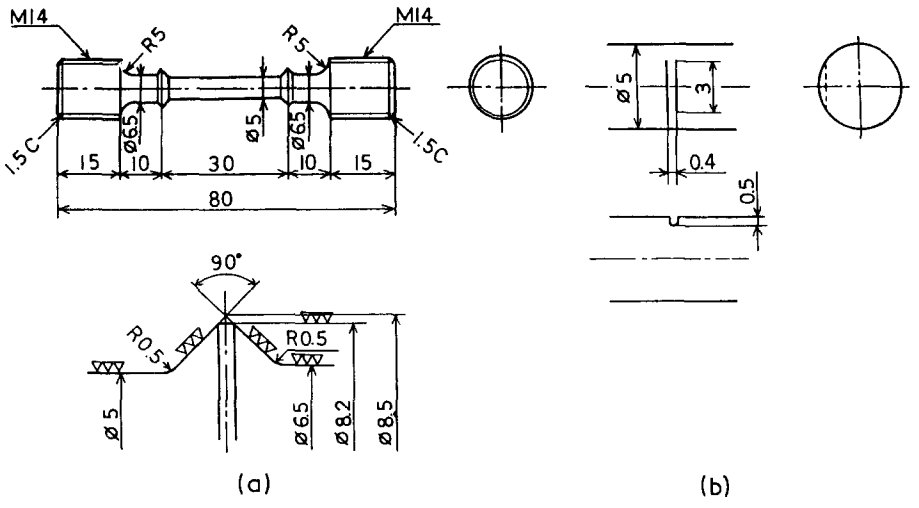

Figure 2 Configurations of specimens for (a) creep and creep-rupture tests and (b) surface crack propagation experiments. Dimensions in millimetres.

is also longer in the steel with strong grain boundaries.

Fig. 6 also shows the creep curves of these steels at 900° C. The tertiary creep occupies a very large portion of the creep curve even under low stresses at temperature above 900° C, irrespective of the grain-boundary configuration of the steel. Grain-boundary cracks occur at a small creep strain in the tertiary creep regime in both the steels at 900° C compared with these cracks at 700° C. The cracks are nucleated at the time of about 50 to 70% of rupture life in the steel with serrated grain boundaries, while they are initiated at about 70 to 80% of it in the one with straight grain boundaries.

Thus, serrated grain boundaries seem to retard the creep crack propagation of steels at 900° C, although creep cracks occurred at small strains. This fact implies that the stress concentrations built up at the triple junctions by grain-boundary sliding are decreased by enhanced diffusion of atoms at very high temperatures to the levels which do not cause triple-point cracking [10, 15]. Further, severe oxidation may affect grain-boundary crack initiation at high temperatures. These factors may lead to the transformation of the mechanism of grain-boundary crack initiation from triple-point cracking [11, 13, 14] to other mechanisms [10, 11, 16].

Even at high temperatures above 900° C, the resistance of steels to creep crack propagation may be improved by the strengthening of grain boundaries.

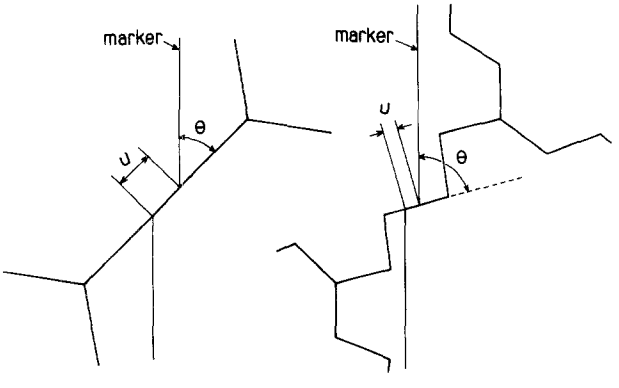

Figure 3 Schematic illustrations of the measurement of grain-boundary sliding: (a) normal straight grain boundary, (b) serrated grain boundary. u = amount of grain-boundary sliding, θ = orientation.

Fig. 7 shows the relation between surface crack propagation rate and surface crack length for steels during creep at 900° C and 27.4 MPa. The crack propagation rate of Steel S with serrated grain boundaries is less than half that of Steel N with straight grain boundaries. The difference in crack propagation rate of these steels is larger when the surface crack length is shorter. Thus, the enhancement of grain-boundary crack propagation resistance (probably due to the deflection of crack paths) is the working mechanism for strengthening by serrated grain boundaries at temperatures above about 900° C.

3.2. Initiation of grain-boundary cracks and grain-boundary fracture

Fig. 8 shows the grain-boundary cracks initiated on the specimen surface during creep at 700 and 900° C. The tensile direction is vertical in the photographs. Small grain-boundary cracks with sizes of less than a few grain diameters are initiated on both the steel with serrated grain boundaries (Fig. 8a) and that with straight grain boundaries (Fig. 8b) at 700° C. These cracks are considered to be nucleated at grain-boundary triple junctions by grain-boundary sliding

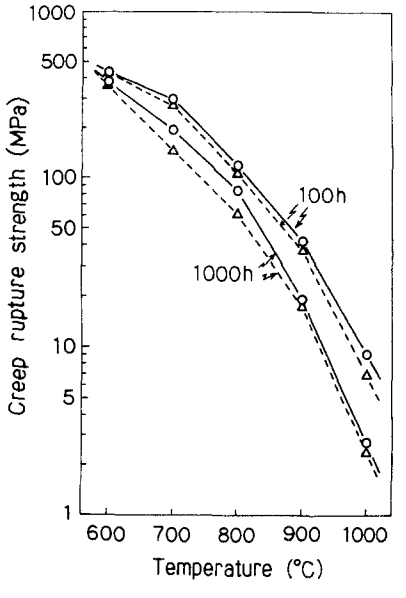

Figure 4 Temperature dependence of creep rupture strength in 21Cr–4Ni–9Mn steels: (○) Steel S, (△) Steel N.

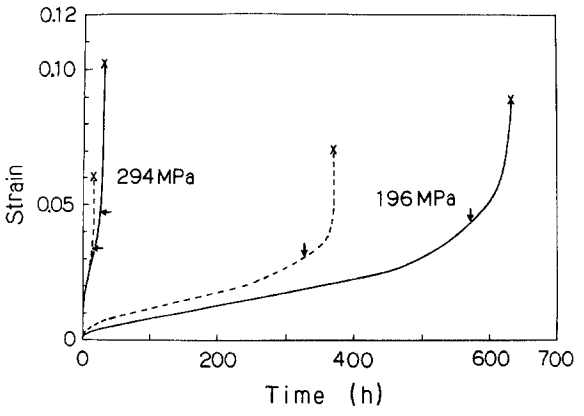

Figure 5 Creep curves of 21Cr–4Ni–9Mn steels at 700° C: (——) Steel S, (– – –) Steel N. Arrows indicate crack initiation.

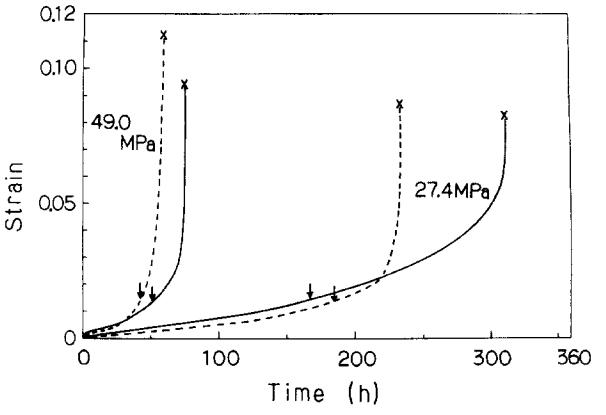

Figure 6 Creep curves of 21Cr–4Ni–9Mn steels at 900° C: (——) Steel S, (– – –) Steel N. Arrows indicate crack initiation.

in both the steels [12–14]. Microvoids also occur in addition to microcracks at 900° C (Figs 8c and d).

Fig. 9 shows the microstructures and fracture surfaces of specimens creep-ruptured at 700° C and 196 MPa. The tensile direction is horizontal in the optical micrographs. Short grain-boundary cracks are visible at grain-boundary triple junctions in Steel S (Fig. 9a), while a long crack is observable in Steel N (Fig. 9b). The fracture surface of the specimen with serrated grain boundaries consists of grain-boundary facets which contain steps and ridges corresponding to serrated grain boundaries and dimple patterns (Figs 9c and e), but that of the specimen with straight grain boundaries shows typical grain-boundary fracture facets (Figs 9d and f).

Fig. 10 shows microstructures and fracture surfaces of specimens creep-ruptured at 900° C and 27.4 MPa. Many microcracks and microvoids are visible near the fracture surface in both specimens (Figs 10a and b). The tensile direction is also horizontal in these optical micrographs. The fracture surface becomes relatively featureless by severe oxidation and surface diffusion of atoms in both the steels at 900° C (Figs 10c and d), except for the trace of nucleation of grain-boundary voids (Fig. 10e) and round grain-boundary facets (Fig. 10f). The microstructures and fracture appearances at 1000° C are almost identical to those at 900° C. Thus, the available information on strengthening by serrated grain boundaries in the crack propagation process could not be obtained by fractography on the specimens creep-ruptured at very high temperatures.

3.3. Effects of grain-boundary configuration on the grain-boundary sliding during creep at 700° C

Fig. 11 shows the grain-boundary sliding observed on specimens with serrated grain boundaries (Steel S) and those with straight grain boundaries (Steel N) during creep at 700° C. As is expected, the average amount of grain-boundary sliding considerably decreases by strengthening of grain boundaries. Horton [17] also confirmed the retardation of grain-boundary sliding by second-phase particles in an Al–Fe alloy. The change in the average amount of sliding with time is similar to the shape of creep curve generated under the same creep conditions (Fig. 5). The fraction of sliding grain boundaries relative to total grain boundaries increased with time irrespective of the grain-boundary configuration. However, this fraction is at most 30% in specimens with straight grain boundaries, although it is larger in specimens with straight grain boundaries than in those with serrated grain boundaries. Fig. 12 shows grain boundaries of specimens crept to about 4% strain. The off-sets of marker lines due to grain-boundary sliding are too small to confirm at low magnification (Figs 12a and b). Even at higher magnifications, the grain-boundary sliding is difficult to confirm in Steel S with serrated grain boundaries (Fig. 12c), while it is discernible in Steel N with straight grain boundaries (Fig. 12d).

Fig. 13 shows the relation between the average amount of grain-boundary sliding and creep strain in specimens during creep at 700° C. The amount of the sliding in each specimen increases with creep strain. The amount of it in specimens with serrated grain boundaries is less than one-third of that in those with straight grain boundaries at the identical creep strain under the same creep conditions. The amount of sliding to crack initiation is also indicated by arrows in the figure. This critical amount of sliding is larger in the steel with straight grain boundaries than in that with serrated grain boundaries. This value is slightly

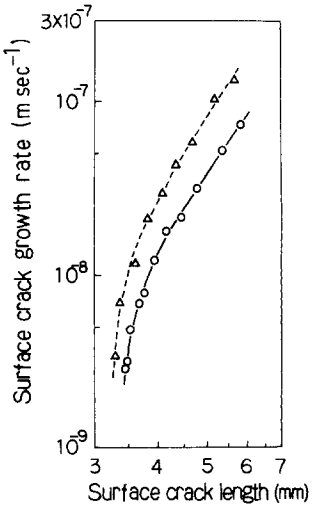

Figure 7 The effect of grain-boundary strengthening on the surface crack propagation rate of 21Cr–4Ni–9Mn steels during creep at 900° C and 27.4 MPa: (○) Steel S, (△) Steel N.

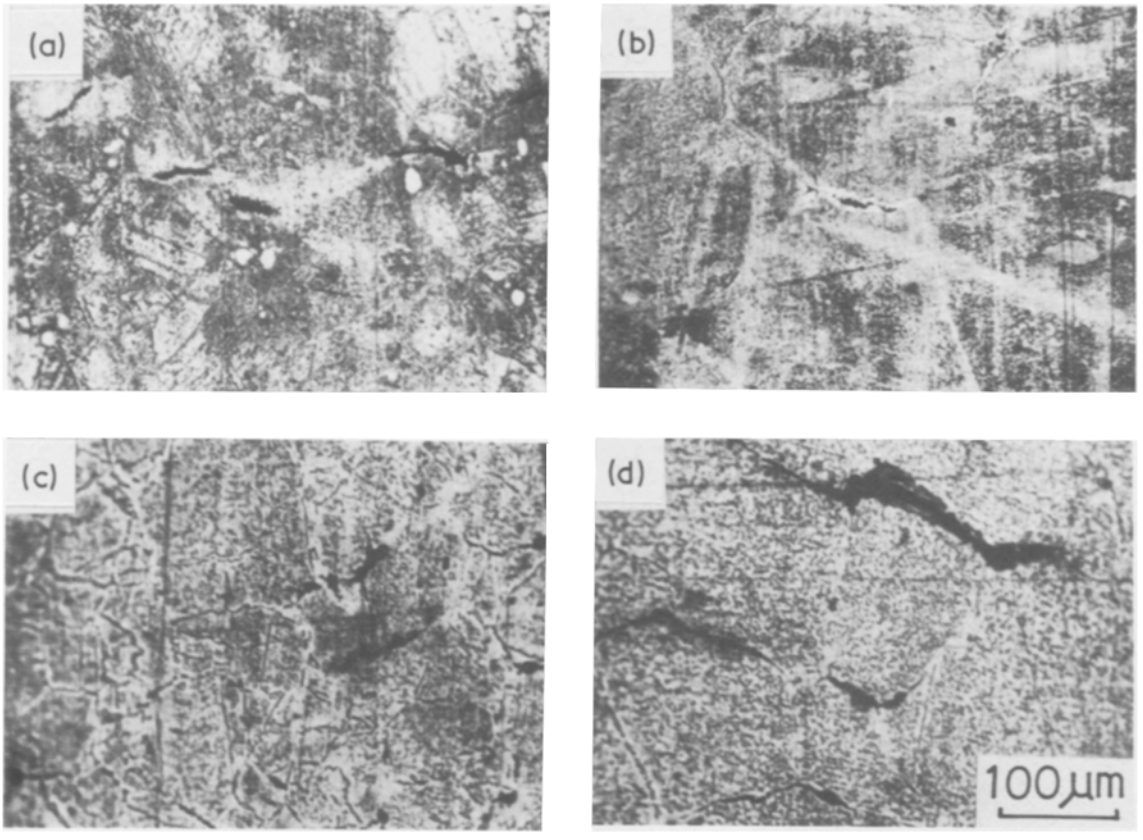

Figure 8 Grain-boundary cracks observed on 21Cr–4Ni–9Mn steels with two types of grain-boundary configurations. (a) Steel S (700° C, 196 MPa, 0.99 tr); (b) Steel N (700° C, 196 MPa, 0.94 tr); (c) Steel S (900° C, 27.4 MPa, 0.68 tr); (d) Steel S (900° C, 27.4 MPa, 0.94 tr) (tr: rupture life).

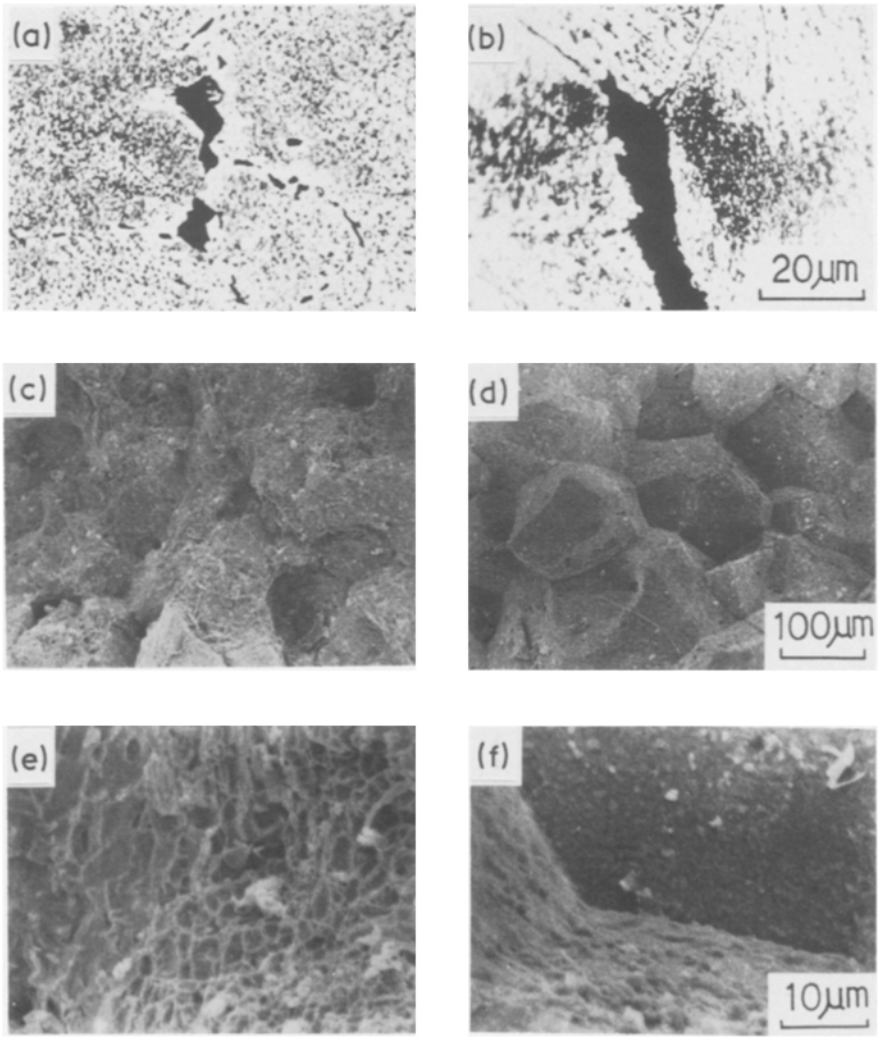

Figure 9 Optical and scanning electron micrographs of 21Cr–4Ni–9Mn steels creep-ruptured at 700° C, 196 MPa. (a, c, e) Steel S; (b, d, f) Steel N.

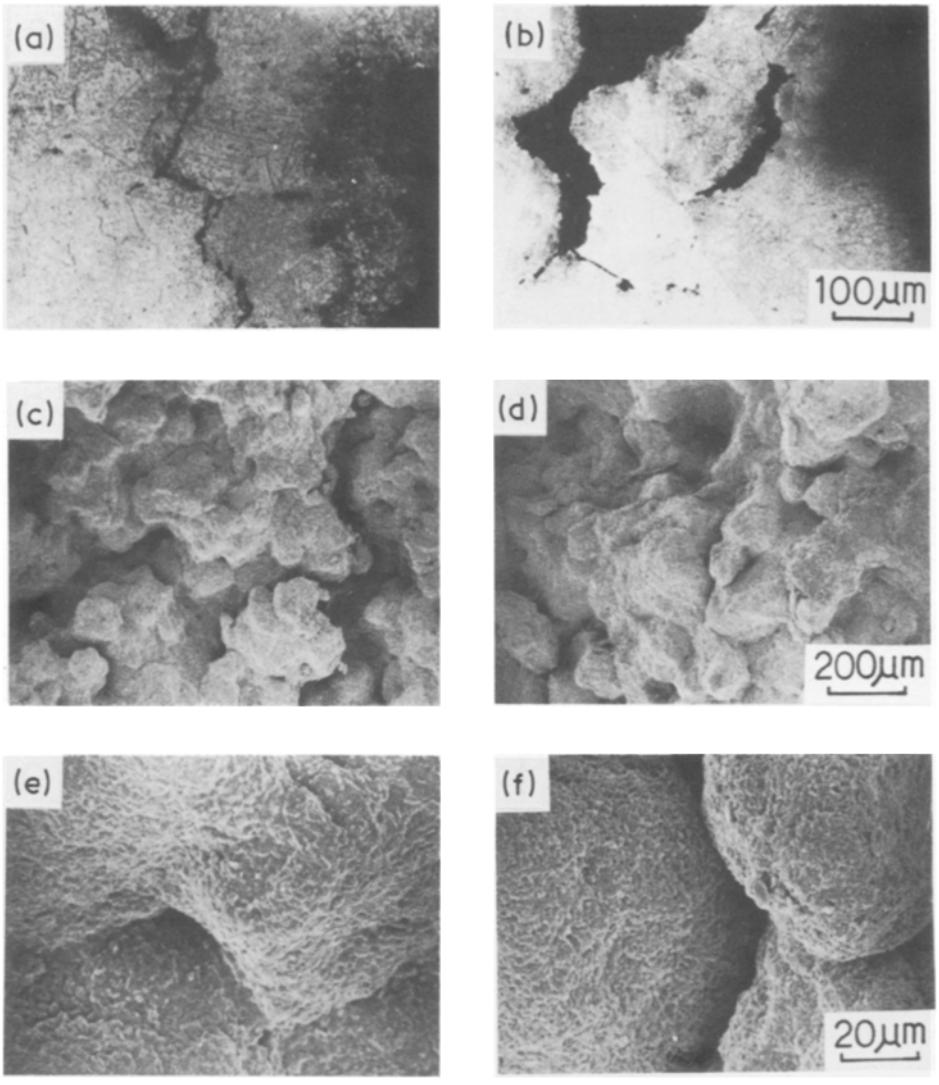

Figure 10 Optical and scanning electron micrographs of 21Cr–4Ni–9Mn steels creep-ruptured at 900° C, 27.4 MPa. (a, c, e) Steel S; (b, d, f) Steel N.

larger when the applied stress is lower. The amount of grain-boundary sliding is slightly larger under the lower stress (196 MPa), irrespective of the grain-boundary configurations in specimens.

Fig. 14 shows the relation between the amount of sliding of each grain boundary and the orientation difference between the boundary and the tensile direction (θ) in specimens crept to about 4% strain at 700° C and 294 MPa. The average amount of the sliding ($\bar{u}$) is also shown in the figure. The grain-boundary sliding occurs on grain boundaries with the orientation difference (θ) more than about 30°, and the amount of it has a maximum value of θ in the range from 60 to 70° in both specimens.

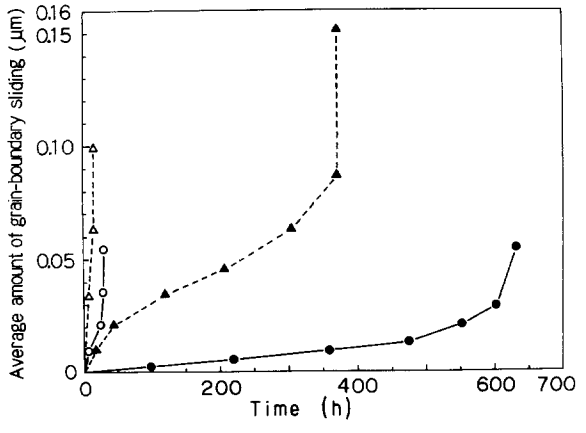

Figure 11 The average amount of grain-boundary sliding in 21Cr–4Ni–9Mn steels with two types of grain boundary configuration during creep at 700° C. (●) Steel S, 196 MPa; (○) Steel S, 294 MPa; (▲) Steel N, 196 MPa; (△) Steel N, 294 MPa.

Fig. 15 shows the stress dependence of average grain-boundary sliding rate in the steady-state creep regime at 700° C. The sliding rate of specimens ($\dot{\bar{u}}$) with serrated grain boundaries is less than one-third of that of specimens with straight grain boundaries. The stress exponent (m) is 6.5 for the former and 6.7 for the latter when these data points are fitted to a power law ($\dot{\bar{u}} \propto \sigma^m$). Fig. 16 shows the stress dependence of steady-state creep rate ($\dot{\varepsilon}_s \propto \sigma^n$), although the values of the creep rate are almost the same in these two kinds of steel. The stress dependence of grain-boundary sliding rate is slightly lower than that of the steady-state creep rate in these steels. These experimental results coincide with those reported by other investigators on several kinds of metallic material [18].

4. Conclusions

The effect of grain-boundary strengthening on the creep-rupture strength by modification of the grain-boundary configuration has been investigated using austenitic 21Cr–4Ni–9Mn engine-valve steel in a wide temperature range from 600 to 1000° C in air.

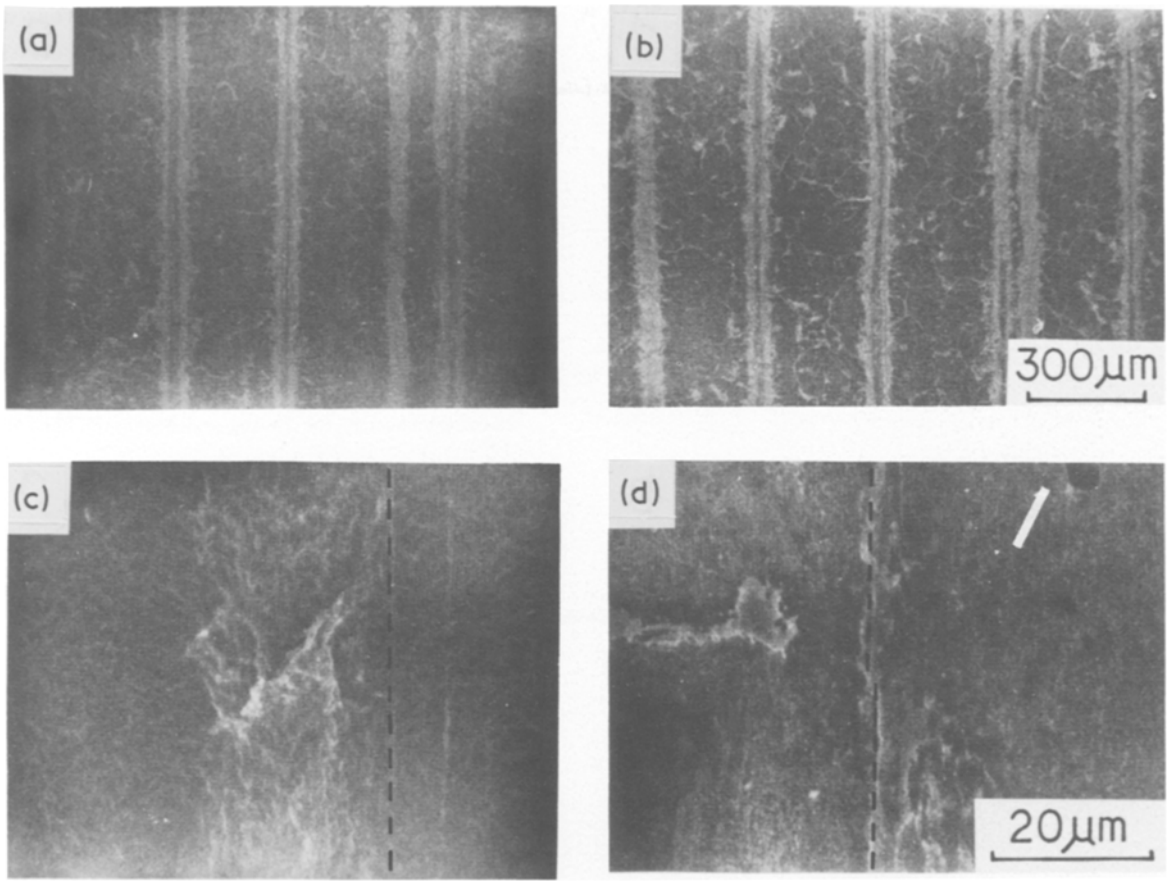

Figure 12 An example of grain-boundary sliding in 21Cr–4Ni–9Mn steels during creep at 700° C. (a, b) markers on the specimen surface; (c, d) off-set of a marker. (a, c) Steel S; (b, d) Steel N (creep strain = 0.04).

Further, grain-boundary sliding was also examined on a steel with serrated grain boundaries during creep at 700° C. The results obtained are summarized as follows.

1. The improvement of creep-rupture strength by the strengthening of grain boundaries was observed at temperatures above 600° C. The 1000 h rupture strength of a steel with serrated grain boundaries was relatively higher than that of the steel with straight grain boundaries, especially at 700 and 800° C.

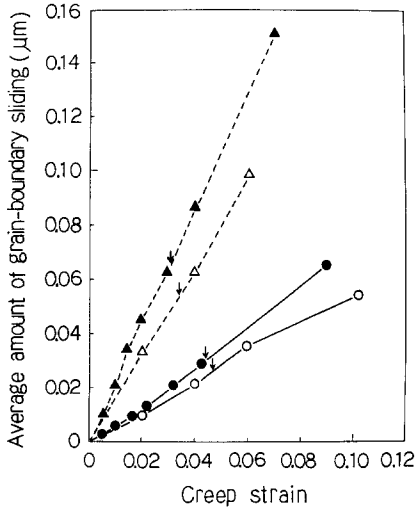

Figure 13 The relation between the average amount of grain-boundary sliding and total creep strain in 21Cr–4Ni–9Mn steels at 700° C. (●) Steel S, 196 MPa; (○) Steel S, 294 MPa; (▲) Steel N, 196 MPa; (△) Steel N, 294 MPa. Arrows indicate crack initiation.

2. The strengthening of heat-resisting steel by serrated grain boundaries was effective in retarding both the crack initiation and the final creep rupture of the steel at temperatures around 700° C, while it only increased the resistance to creep crack propagation at temperatures above about 900° C. This may be caused by severe oxidation and the surface diffusion of atoms, which lead to a change in the crack initiation mechanism with increasing test temperature.

3. Grain-boundary sliding was considerably inhibited by the strengthening of grain boundaries at 700° C. The average amount of it in a steel with serrated grain boundaries was less than about one-third of that of the steel with straight grain boundaries at

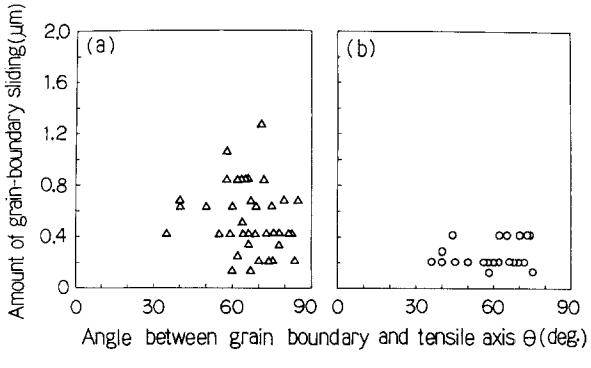

Figure 14 The relation between the average amount of grain-boundary sliding and the grain-boundary orientation in 21Cr–4Ni–9Mn steels at 700° C and 294 MPa; $\varepsilon = 0.04$. (a) Steel N: $\bar{u} = 6.29 \times 10^{-2}\,\mu m$, $t = 15.2$ h. (b) Steel S: $\bar{u} = 2.13 \times 10^{-2}\,\mu m$, $t = 24.5$ h.

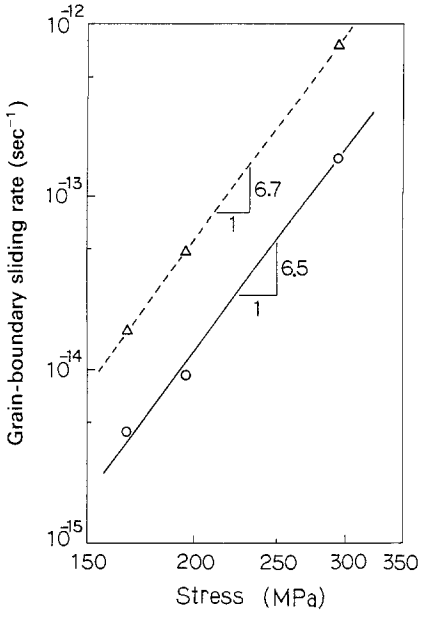

Figure 15 The stress dependence of average grain-boundary sliding rate in the steady-state creep regime in 21Cr–4Ni–9Mn steels at 700° C: (○) Steel S, (△) Steel N.

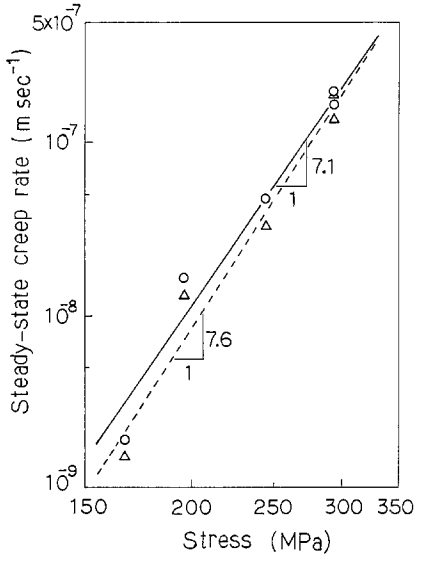

Figure 16 The stress dependence of steady-state creep rate in 21Cr–4Ni–9Mn steels during creep at 700° C: (——, ○) Steel S; (– – –, △) Steel N.

the same creep strain. The amount of the sliding at the same creep strain was larger at lower stress in the same steel. It was dependent of the orientation of each grain boundary. The fraction of sliding grain boundaries relative to total grain boundaries was less than about 30%. The stress dependence of grain-boundary sliding in the two types of steel in the steady-state regime was almost identical, and was slightly less than that of the steady-state creep rate.

References

1. M. YAMAZAKI, *J. Jpn Inst. Metals* **30** (1966) 1032.
2. J. C. RUNKLE and R. M. PELLOUX, ASTM STP 675 (American Society for Testing and Materials, Philadelphia, 1979) p. 501.
3. W. BETTERIDGE and A. W. FRANKLIN, *J. Inst. Metals* **85** (1956–57) 473.
4. V. LUPINC, "High Temperature Alloys for Gas Turbines 1982" (Reidel, Dordrecht, 1982) p. 395.
5. M. KOBAYASHI, O. MIYAGAWA and M. YAMAMOTO, in Proceedings of International Conference on Creep, Tokyo, April 1986, edited by H. Udoguchi *et al.* (Japanese Society for Mechanical Engineers, Tokyo, 1986) p. 65.
6. T. SAGA, O. MIYAGAWA, M. KOBAYASHI and D. FUJISHIRO, *Trans. Iron Steel Inst. Jpn* **58** (1972) 859.
7. A. K. KOUL and GESSINGER, *Acta Metall.* **31** (1983) 1061.
8. M. YAMAMOTO, O. MIYAGAWA, M. KOBAYASHI and D. FUJISHIRO, *Trans. Iron Steel Inst. Jpn* **63** (1977) 1848.
9. M. TANAKA, O. MIYAGAWA, T. SAKAKI and D. FUJISHIRO, *ibid.* **65** (1979) 939.
10. M. TANAKA and H. IIZUKA, in Proceedings of International Conference on Creep, Tokyo, April 1986, edited by H. Udoguchi *et al.* (Japanese Society for Mechanical Engineers, Tokyo, 1986) p. 187.
11. D. McLEAN, *J. Inst. Metals* **85** (1956–57) 468.
12. S. TAIRA, M. FUJINO and M. YOSHIDA, *J. Soc. Mater. Sci. Jpn* **27** (1978) 447.
13. J. A. WILLIAMS, *Acta Metall.* **15** (1967) 1119.
14. T. G. LANGDON, *Phil. Mag.* **23** (1970) 945.
15. R. RAJ, *Trans. ASME, Ser. H* **43** (1976) 132.
16. W. BEERE and M. V. SPEIGHT, *Metal Sci.* **12** (1978) 593.
17. C. P. A. HORTON, *Acta Metall.* **20** (1972) 477.
18. T. G. LANGDON and R. B. VASTAVA, ASTM STP 765 (American Society for Testing and Materials, Philadelphia, 1982) p. 435.

Received 15 April
and accepted 6 July 1987